PERGAMON

International Journal of Solids and Structures 40 (2003) 6681–6702

INTERNATIONAL JOURNAL OF SOLIDS and STRUCTURES

www.elsevier.com/locate/ijsolstr

From particle ensembles to Cosserat continua: homogenization of contact forces towards stresses and couple stresses

W. Ehlers [a,*], E. Ramm [b], S. Diebels [c], G.A. D'Addetta [b]

[a] Institut für Mechanik (Bauwesen), Universität Stuttgart, Pfaffenwaldring 7, 70550 Stuttgart, Germany
[b] Institut für Baustatik, Universität Stuttgart, 70550 Stuttgart, Germany
[c] Lehrstuhl für Technische Mechanik, Universität des Saarlandes, 66123 Saarbrücken, Germany

Received 28 January 2003; received in revised form 23 June 2003

Abstract

In the present contribution, a transition from the dynamics of single particles to a Cosserat continuum is discussed. Based on the definition of volume averages, expressions for the macroscopic stress tensors and for the couple stress tensors are derived. It is found that an ensemble of particles allows for a non-symmetric macroscopic stress tensor and, thus, for the existence of couple stresses, even if the single particles are considered as standard continua. Discrete element method simulations of a biaxial box are used for the validation of the proposed homogenization technique.

Keywords: Rigid body dynamics; Cosserat continuum; Homogenization procedure; Stress and couple stress tensors

1. Introduction

The theoretical description of granular media is a challenging task and is required in several branches of engineering such as geotechnics and soil mechanics but also in various technological applications such as powder technologies or sintering processes. Basically, granular media can be treated by two different approaches proceeding either from microscopic or from macroscopic considerations. While the microscopic approach is based on the description of the single grain behaviour of the granular medium by use of rigid body dynamics, the macroscopic approach depends on continuum mechanical methods. The advantage of the microscopic approach lies, on the one hand, in the simplicity of formulating constitutive equations for the particle contacts and, on the other hand, in the detection of any kind of oncoming localization during the deformation process. However, treating realistic boundary-value problems stemming from engineering requirements implies the necessity of solving a huge amount of coupled equations, where the motion of billions of particles has to be described, e.g., on the basis of the discrete element method (DEM),

* Corresponding author.
E-mail address: ehlers@mechbau.uni-stuttgart.de (W. Ehlers).

0020-7683/$ - see front matter © 2003 Elsevier Ltd. All rights reserved.
doi:10.1016/S0020-7683(03)00418-9

cf., e.g., the work by Cundall and Strack (1979). If one proceeds from continuum mechanics, where the granular medium can be described as a porous solid material rather than an ensemble of particles, the number of equations that has to be solved is generally much smaller. As a consequence, one obtains a more convenient solution procedure for the treatment of realistic boundary-value problems, e.g., on the basis of the finite element method (FEM), cf., e.g., the work by Ehlers and Volk (1998), Ehlers et al. (2001b) and Ehlers (2002). On the other hand, the macroscopic constitutive description of granular materials is highly complex combining elastic, plastic and viscous material properties. Furthermore, it is well known that, if localization phenomena occur, the mathematical problem becomes ill-posed and has to be regularized. Following this, the continuum mechanical solution of boundary-value problems, where localization phenomena are expected, has to include a regularization mechanism, which, in the frame of granular media, is naturally given by taking into account a micropolar or a Cosserat continuum (Ehlers and Volk, 1998), respectively. Note in passing that a link between the Cosserat continuum and localization phenomena has firstly been made by Mühlhaus and Vardoulakis (1987). Concerning a general view on a continuum bifurcation analysis of geomaterials, the reader is referred to the work by Brinkgreve (1994) or by Vardoulakis and Sulem (1995).

Apart from considering either the microscopic or the macroscopic approach to granular media, there is a convenient possibility to combine the advantages of both strategies. In particular, this method is given by a continuum mechanical treatment of granular materials on the macroscale, where the constitutive description, e.g., the relation between stresses and strains, is substituted by the solution of a microscopic problem based on particle mechanics. The result obtained by solving the underlying problem on the microscale can then be homogenized by volume averages, thus relating, e.g., particle contact forces to macroscopic stresses. Following this, it is one of the key points of the present contribution to deliver a homogenization strategy, where macroscopic quantities are obtained as volume averages taken over the microstructure. In contrast to the standard literature, where the homogenized stresses are usually assumed to be symmetric, cf., e.g., the work by Drescher and de Josselin de Jong (1972) and follow-up papers, the present findings also reveal stress asymmetries accompanied by couple stresses. These findings are due to the fact that three different scales are considered, namely, the microscale on the grain level, the mesoscale understood as the scale of the representative elementary volume (REV) and the macroscale of the total granular ensemble under study. It is furthermore considered that the systems to be investigated on the different scales are of completely different size, thus allowing for the application of Hashin's MMM principle of scale separation (Hashin, 1983). However, the question of how large the REVs under consideration must be has been extensively discussed in the literature, cf., e.g., the work by Bear and Bachmat (1991) or by Nemat-Nasser and Hori (1999). This question is of considerable importance, since a homogenization procedure always filters the information obtained on the underlying scale. Thus, the size of the REVs must be chosen in such a way that, on the one hand, the homogenized quantities represent convenient substitutes of their counterparts on the microscale and that, on the other hand, the homogenization process does not smear out local effects like stress and strain localizations within shear bands.

Following the above remarks, it is the goal of the present contribution to answer the question of how large must a typical REV be chosen to meet the above requirements. This question will be treated on the basis of the DEM in combination with homogenization strategies, where the forces of the particle network are related to macroscopic stresses and couple stresses. In particular, the paper starts with a brief reconsideration of the basic axioms of rigid body dynamics and of continuum mechanics, where both non-polar and micropolar media are taken into account. In a second step, single particles are considered which are embedded in the granular medium. In full agreement with the literature (Drescher and de Josselin de Jong, 1972; Cundall et al., 1982), the particle stresses computed from contact forces are found symmetric. However, taking into account an ensemble of particles considered as the REV and embedded in a granular medium reveals that the ensemble is governed by non-symmetric stresses in addition to couple stresses. These findings are due to the fact that the particle contact forces are reduced to the particle mass centers,

thus yielding both a particle force resultant and a particle moment resultant, where the latter turns out to govern the existence of couple stresses. The following homogenization procedure relates the force and moment resultants of the particles included in the REV to average stresses and couple stresses representing the macroscopic counterparts of the local REV behaviour, cf. Diebels and Ehlers (2001), Diebels et al. (2001) and Ehlers et al. (2001a).

In order to verify the proposed averaging strategy, a DEM simulation (Tillemans and Herrmann, 1995; Kun and Herrmann, 1996; D'Addetta et al., 2002) of the well-known biaxial test is carried out, where the homogenization procedure is numerically applied to the contact force network. As is well-known from both experiments (Viggiani et al., 2001) and FEM computations of the biaxial test based on continuum mechanical considerations in the frame of granular media (Ehlers and Volk, 1998), it is expected that, at the beginning of the deformation process, a fully homogeneous situation occurs which is followed by a strain localization procedure, where narrow shear bands can be found. Furthermore, the numerical computations by Ehlers and Volk (1998) revealed that the evolving shear bands are strongly affected by micropolar grain rotations and couple stresses. In the present contribution, it is shown by use of different REV sizes that sufficiently small REVs can resolve the oncoming localizations by representing the couple stresses and stress asymmetries, whereas increasing the size of the REVs or increasing the ratio between the REV volumes and the REV surfaces, respectively, eliminates these effects. This result is not surprising, since it is known from experiments that the shear band width covers only a very few grain diameters (Viggiani et al., 2001). Consequently, if the REV is large compared to the shear band thickness, the local inhomogeneities are fully smeared out. Similar results have recently been found by Bardet and Vardoulakis (2001), where it has been shown on the basis of a homogenization strategy proceeding from the virtual work principle that stress asymmetries and couple stresses can basically arise. It has furthermore been shown that these asymmetries decrease with an increasing ratio between the volume and the surface of the particle ensemble under study.

2. Momentum and angular momentum of single particles

This section briefly recalls the basic results of rigid body dynamics as well as of mechanics of deformable continua. These results are the onset of the homogenization process applied to single particles and to ensembles of particles in order to compute macroscopic stresses and couple stresses from a given distribution of contact forces.

The mass of a single particle $\mathscr{P}$, rigid or deformable, is given by

$$m = \int_{\mathscr{P}} \mathrm{d}m = \int_{\mathscr{P}} \rho \, \mathrm{d}v, \tag{1}$$

where $\mathrm{d}m$ is the mass element, ρ the mass density and $\mathrm{d}v$ the volume element of $\mathscr{P}$.

If $\mathscr{P}$ is considered as a rigid particle of arbitrary shape, the motion of $\mathscr{P}$ is described by the translation of its center of mass and by the rotation around it. The position $\mathbf{x}_M$ of the center of mass M of the particle is defined by

$$\mathbf{x}_M = \frac{1}{m} \int_{\mathscr{P}} \mathbf{x} \, \mathrm{d}m, \tag{2}$$

cf. Fig. 1, where $\mathbf{x}_M$ is equivalent to the volume center $\mathbf{x}_V$ of $\mathscr{P}$ in case of homogeneous density distributions. Furthermore, the introduction of a local position vector

$$\bar{\mathbf{x}} = \mathbf{x} - \mathbf{x}_M \tag{3}$$

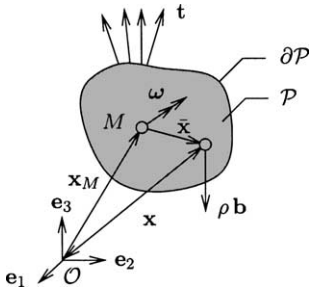

Fig. 1. Forces acting on a single particle $\mathscr{P}$ with boundary $\partial\mathscr{P}$.

relative to M includes the identity

$$\int_{\mathscr{P}} \bar{\mathbf{x}}\,\mathrm{d}m = \mathbf{0}. \tag{4}$$

Applying the axioms of mechanics to an arbitrary particle $\mathscr{P}$, rigid or deformable, the balance of momentum (linear momentum) yields

$$\dot{\mathbf{p}} := \frac{\mathrm{d}}{\mathrm{d}t}\mathbf{p} = \mathbf{k}, \tag{5}$$

where the momentum $\mathbf{p}$ and the external forces $\mathbf{k}$ are given by

$$\mathbf{p} = \int_{\mathscr{P}} \dot{\mathbf{x}}\,\mathrm{d}m, \quad \mathbf{k} = \int_{\partial\mathscr{P}} \mathbf{t}\,\mathrm{d}a + \int_{\mathscr{P}} \mathbf{b}\,\mathrm{d}m. \tag{6}$$

Therein, $\mathbf{t}$ represents the external stress vector (contact forces per surface element $\mathrm{d}a$), whereas $\mathbf{b}$ indicates the body forces (gravitation) per mass element $\mathrm{d}m$. In case of particle mechanics, where $\mathscr{P}$ is assumed to be a rigid body rather than a deformable continuum, one is generally not interested in a local but only in a global statement. Following this, one obtains the global momentum balance with respect to M with the aid of (3), (5) and (6) via

$$m\ddot{\mathbf{x}}_M = \mathbf{k}. \tag{7}$$

In continuum mechanics, where $\mathscr{P}$ is usually assumed to be a deformable body, the combination of (5) and (6) yields

$$\int_{\mathscr{P}} \rho\ddot{\mathbf{x}}\,\mathrm{d}v = \int_{\mathscr{P}} (\operatorname{div}\mathbf{T} + \rho\mathbf{b})\,\mathrm{d}v, \tag{8}$$

where $\mathbf{T}$ is the Cauchy stress tensor related to the surface tractions by $\mathbf{t} = \mathbf{T}\mathbf{n}$ ($\mathbf{n}$ is the outward oriented unit surface normal), and $\operatorname{div}(\cdot)$ is the divergence operator corresponding to the gradient operator $\operatorname{grad}(\cdot)$ taken with respect to the spatial position $\mathbf{x}$. Furthermore, if the fields incorporated in (8) are steady and sufficiently often steadily differentiable, the local form of the momentum balance reads

$$\rho\ddot{\mathbf{x}} = \operatorname{div}\mathbf{T} + \rho\mathbf{b}. \tag{9}$$

No matter if $\mathscr{P}$ is rigid or deformable, the balance of angular momentum (moment of momentum) is defined with respect to an arbitrary but fixed point in space which, in the present study, is chosen without loss of generality as the spatial origin $\mathscr{O}$. Thus,

$$\dot{\mathbf{h}}_0 := \frac{\mathrm{d}}{\mathrm{d}t}\mathbf{h} = \mathbf{m}_0, \tag{10}$$

where the angular momentum vector $\mathbf{h}_0$ and the moments $\mathbf{m}_0$ of the external forces are given by

$$\mathbf{h}_0 = \int_{\mathscr{P}} \mathbf{x} \times \dot{\mathbf{x}}\,\mathrm{d}m, \quad \mathbf{m}_0 = \int_{\partial\mathscr{P}} \mathbf{x} \times \mathbf{t}\,\mathrm{d}a + \int_{\mathscr{P}} \mathbf{x} \times \mathbf{b}\,\mathrm{d}m. \tag{11}$$

In case of rigid body dynamics, a substitution of $\mathbf{x}$ by $\mathbf{x}_M + \bar{\mathbf{x}}$ yields the angular momentum and the moment of the external forces via

$$\mathbf{h}_0 = \mathbf{x}_M \times m\dot{\mathbf{x}}_M + \mathbf{h}_M, \quad \mathbf{m}_0 = \mathbf{x}_M \times \mathbf{k} + \mathbf{m}_M, \tag{12}$$

where

$$\mathbf{h}_M = \int_{\mathscr{P}} \bar{\mathbf{x}} \times \dot{\bar{\mathbf{x}}}\,\mathrm{d}m, \quad \mathbf{m}_M = \int_{\partial\mathscr{P}} \bar{\mathbf{x}} \times \mathbf{t}\,\mathrm{d}a + \int_{\mathscr{P}} \bar{\mathbf{x}} \times \mathbf{b}\,\mathrm{d}m \tag{13}$$

define the angular momentum and the moments of $\mathscr{P}$ with respect to M. Note in passing that the second term of $(13)_2$ generally vanishes, since the center of gravitation and the center of mass coincide, if $\mathbf{b}$ is constant and is, thus, independent of $\mathbf{x}$. Taking into account that $\mathscr{P}$ is assumed as a rigid body, where the norm $|\bar{\mathbf{x}}|$ of the position vectors $\bar{\mathbf{x}}$ relative to M is constant, the corresponding velocities $\dot{\bar{\mathbf{x}}}$ are obtained via

$$\dot{\bar{\mathbf{x}}} = \boldsymbol{\omega} \times \bar{\mathbf{x}} =: \boldsymbol{\Omega}\bar{\mathbf{x}}. \tag{14}$$

Therein, $\boldsymbol{\omega}$ is the angular velocity of the rigid body motion and $\boldsymbol{\Omega}$ the corresponding skew-symmetric gyration tensor:

$$\boldsymbol{\Omega} = -\overset{3}{\mathbf{E}}\boldsymbol{\omega} \leftrightarrow \boldsymbol{\omega} = -\frac{1}{2}\overset{3}{\mathbf{E}}\boldsymbol{\Omega} = \frac{1}{2}\overset{3}{\mathbf{E}}\boldsymbol{\Omega}^{\mathrm{T}}. \tag{15}$$

Note in passing that $\overset{3}{\mathbf{E}}$ defines the fundamental tensor of third order (*Ricci* permutation tensor) and that $\boldsymbol{\omega}$ is the axial vector of $\boldsymbol{\Omega}$. By combination of $(13)_1$ and (14), $\mathbf{h}_M$ is obtained as

$$\mathbf{h}_M =: \boldsymbol{\Theta}_M\boldsymbol{\omega}, \tag{16}$$

where

$$\boldsymbol{\Theta}_M = \int_{\mathscr{P}} [(\bar{\mathbf{x}} \cdot \bar{\mathbf{x}})\mathbf{I} - (\bar{\mathbf{x}} \otimes \bar{\mathbf{x}})]\,\mathrm{d}m \tag{17}$$

defines the positive definite, symmetric mass tensor of inertia, where $\mathbf{I}$ is the fundamental tensor of second order (identity tensor). Consideration of (7) and (13) together with the above results yields the angular momentum balance with respect to M via

$$\dot{\mathbf{h}}_M = \mathbf{m}_M \quad \text{or} \quad (\boldsymbol{\Theta}_M\boldsymbol{\omega})^{\cdot} = \mathbf{m}_M, \tag{18}$$

respectively, where

$$(\boldsymbol{\Theta}_M\boldsymbol{\omega})^{\cdot} = \dot{\boldsymbol{\Theta}}_M\boldsymbol{\omega} + \boldsymbol{\Theta}_M\dot{\boldsymbol{\omega}}. \tag{19}$$

Therein, the time derivative of $\boldsymbol{\Theta}_M$ can be given by

$$\dot{\boldsymbol{\Theta}}_M = \overset{\diamond}{\boldsymbol{\Theta}}_M + \boldsymbol{\Omega}\boldsymbol{\Theta}_M + \boldsymbol{\Theta}_M\boldsymbol{\Omega}^{\mathrm{T}}, \tag{20}$$

where $\overset{\diamond}{\boldsymbol{\Theta}}_M$ is the Green–Naghdi rate of $\boldsymbol{\Theta}_M$ taken with respect to a co-rotational frame fixed to the mass center M of $\mathscr{P}$. Since $\mathscr{P}$ was assumed as a rigid body with constant values of $|\bar{\mathbf{x}}|$, the Green–Naghdi rate vanishes and (20) reduces to

$$\dot{\boldsymbol{\Theta}}_M = 2\,\mathrm{sym}(\boldsymbol{\Omega}\boldsymbol{\Theta}_M). \tag{21}$$

Given the above results together with (7)–(13), the angular momentum balance of a rigid particle $\mathscr{P}$ can be split into the terms:

$$\begin{aligned} &\mathbf{x}_M \times m\ddot{\mathbf{x}}_M = \mathbf{x}_M \times \mathbf{k}, \\ &\boldsymbol{\Theta}_M \dot{\boldsymbol{\omega}} + 2\,\mathrm{sym}(\boldsymbol{\Omega}\boldsymbol{\Theta}_M)\boldsymbol{\omega} = \mathbf{m}_M. \end{aligned} \tag{22}$$

From the above set of equations, it is seen that only the second relation, which is generally known as Euler's gyration equation, has the property of an axiom, while the first one is a result of the momentum balance. It is furthermore concluded that, in the limit of a particle $\mathscr{P}$ reducing to a material point with vanishing values of $|\bar{\mathbf{x}}|$, both $\mathbf{m}_M$ and the tensor of inertia $\boldsymbol{\Theta}_M$ vanish and only $(22)_1$ remains as an identity.

If the particle $\mathscr{P}$ has to be considered as a deformable rather than a rigid body, the result (22) has to be replaced by a more general approach. Given the axiomatic angular momentum balance (10) together with the information included in (11), the balance equation reads

$$\int_{\mathscr{P}} \mathbf{x} \times \ddot{\mathbf{x}}\,\mathrm{d}m = \int_{\partial\mathscr{P}} \mathbf{x} \times \mathbf{t}\,\mathrm{d}a + \int_{\mathscr{P}} \mathbf{x} \times \mathbf{b}\,\mathrm{d}m. \tag{23}$$

Application of Cauchy's theorem together with the Gaussian integral theorem to the first term of the right hand side of (23) yields

$$\int_{\partial\mathscr{P}} \mathbf{x} \times \mathbf{t}\,\mathrm{d}a = \int_{\partial\mathscr{P}} (\mathbf{x} \times \mathbf{T})\mathbf{n}\,\mathrm{d}a = \int_{\mathscr{P}} \mathrm{div}\,\mathbf{M}\,\mathrm{d}v, \tag{24}$$

where

$$\mathbf{M} := \mathbf{x} \times \mathbf{T} = [\overset{3}{\mathbf{E}}(\mathbf{x} \otimes \mathbf{T})]^{\underline{2}} \tag{25}$$

is defined as the stress moment corresponding to the Cauchy stress $\mathbf{T}$. Note in passing that $[\cdot]^{\underline{2}}$ defines a contraction of the arguments in brackets toward a tensor of second order. Insertion of (24) in (23) yields

$$\int_{\mathscr{P}} \mathbf{x} \times \rho\ddot{\mathbf{x}}\,\mathrm{d}v = \int_{\mathscr{P}} (\mathrm{div}\,\mathbf{M} + \mathbf{x} \times \rho\mathbf{b})\,\mathrm{d}v. \tag{26}$$

From (26), the local angular momentum statement reads

$$\mathbf{x} \times \rho\ddot{\mathbf{x}} = \mathrm{div}\,\mathbf{M} + \mathbf{x} \times \rho\mathbf{b}, \tag{27}$$

where $\mathrm{div}\,\mathbf{M}$ can be split into

$$\mathrm{div}\,\mathbf{M} = \mathbf{I} \times \mathbf{T} + \mathbf{x} \times \mathrm{div}\,\mathbf{T}. \tag{28}$$

Following this and considering the local momentum balance (9) again leads to two different statements of the local form of the balance of angular momentum, namely

$$\begin{aligned} &\mathbf{x} \times \rho\ddot{\mathbf{x}} = \mathbf{x} \times (\mathrm{div}\,\mathbf{T} + \rho\mathbf{b}), \\ &\mathbf{I} \times \mathbf{T} = \mathbf{0}, \end{aligned} \tag{29}$$

where only the second relation includes the axiom of the angular momentum balance, while the first one is an identity resulting from the momentum balance. Finally, it is well known that $(29)_2$ yields

$$\mathbf{0} = \mathbf{I} \times \mathbf{T} = \overset{3}{\mathbf{E}}\mathbf{T}^{\mathrm{T}} = 2\overset{\mathrm{A}}{\mathbf{t}} \rightarrow \mathbf{T} = \mathbf{T}^{\mathrm{T}}, \tag{30}$$

where $\overset{\mathrm{A}}{\mathbf{t}}$ is the axial vector associated with the skew-symmetric part of $\mathbf{T}$. Obviously, the Cauchy stress is symmetric.

However, if a continuous body is considered, by definition, as a Cosserat continuum, the angular momentum $\mathbf{h}_0$ and the external moment $\mathbf{m}_0$ of (11) have to be extended by

$$\begin{aligned}\mathbf{h}_0 &= \int_{\mathscr{P}} (\mathbf{x}\times\dot{\mathbf{x}} + \overline{\boldsymbol{\Theta}}\bar{\boldsymbol{\omega}})\,\mathrm{d}m,\\ \mathbf{m}_0 &= \int_{\partial\mathscr{P}} (\mathbf{x}\times\mathbf{t} + \bar{\mathbf{m}})\,\mathrm{d}a + \int_{\mathscr{P}} (\mathbf{x}\times\mathbf{b} + \mathbf{c})\,\mathrm{d}m.\end{aligned} \tag{31}$$

Therein, $\overline{\boldsymbol{\Theta}}$ is defined as the symmetric tensor of microinertia and $\bar{\boldsymbol{\omega}}$ is understood as the total local rotational velocity given as the result of both the continuum rotation and the independent Cosserat rotation (Ehlers and Volk, 1998). Furthermore, $\bar{\mathbf{m}}$ is the contact moment acting on the boundary of the body under consideration, whereas $\mathbf{c}$ is known as the body couple. Concerning further details on the discussion of Cosserat continua and the application of micropolar media to a variety of boundary-value problems, the interested reader is referred to Ehlers (2002) and Ehlers and Volk (1998) and the quotations therein. Substituting (11) by (31), a combination of (10) and (31) yields the axiom of angular momentum to read

$$\int_{\mathscr{P}} [\mathbf{x}\times\rho\ddot{\mathbf{x}} + \rho(\overline{\boldsymbol{\Theta}}\bar{\boldsymbol{\omega}})^{\cdot}]\,\mathrm{d}v = \int_{\mathscr{P}} [\mathrm{div}(\mathbf{M}+\overline{\mathbf{M}}) + \mathbf{x}\times\rho\mathbf{b} + \rho\mathbf{c}]\,\mathrm{d}v, \tag{32}$$

thus substituting (26). Note in passing that the couple stress tensor $\overline{\mathbf{M}}$ is related to the contact moments $\bar{\mathbf{m}}$ through the Cauchy theorem via

$$\bar{\mathbf{m}} = \overline{\mathbf{M}}\mathbf{n}. \tag{33}$$

Given (32), the corresponding local statement reads

$$\mathbf{x}\times\rho\ddot{\mathbf{x}} + \rho(\overline{\boldsymbol{\Theta}}\bar{\boldsymbol{\omega}})^{\cdot} = \mathrm{div}(\mathbf{M}+\overline{\mathbf{M}}) + \mathbf{x}\times\rho\mathbf{b} + \rho\mathbf{c}. \tag{34}$$

Proceeding from (28) together with the local momentum balance (9) again yields two different statements, namely

$$\begin{aligned}\mathbf{x}\times\rho\ddot{\mathbf{x}} &= \mathbf{x}\times(\mathrm{div}\,\mathbf{T} + \rho\mathbf{b}),\\ \rho(\overline{\boldsymbol{\Theta}}\bar{\boldsymbol{\omega}})^{\cdot} &= \mathbf{I}\times\mathbf{T} + \mathrm{div}\,\overline{\mathbf{M}} + \rho\mathbf{c},\end{aligned} \tag{35}$$

where the second relation includes the axiom of the angular momentum balance in the frame of micropolar continua, thus substituting $(29)_2$. In contrast to $(29)_2$ leading to a symmetric stress $\mathbf{T}$, it is seen from $(35)_2$ that $\mathbf{T}$ is non-symmetric, whenever the continuum is micropolar. It is furthermore concluded that $(35)_2$ compares to $(22)_2$, if the right-hand side of $(35)_2$ is identified with the total local moment by contact and volume terms.

Having recalled these well-known results of rigid body dynamics and mechanics of deformable continua, the same procedure can be applied to particles and ensembles of particles embedded in a surrounding continuum.

3. Balance equations for embedded particles

The results derived above have been given for both rigid and deformable single particles independent of their shape and size. However, in several engineering applications, large ensembles of particles have to be considered, cf. Fig. 2. For example, if a sand heap consisting of millions of sand grains is taken into account in the frame of soil mechanics, one is generally interested in the description of the macroscopic behaviour of the body $\mathscr{B}$ (the granular medium) rather than in the behaviour of the individual grains $\mathscr{P}^{(i)}$. Obviously, the macroscopic scale D of $\mathscr{B}$ is much larger than the characteristic dimension δ of the particles $\mathscr{P}^{(i)}$. Furthermore, since the motion of the particles takes place on a scale $\varepsilon = \delta/D \ll 1$, the balance equations of momentum and of angular momentum of the single particles can be simplified by use of the arguments of

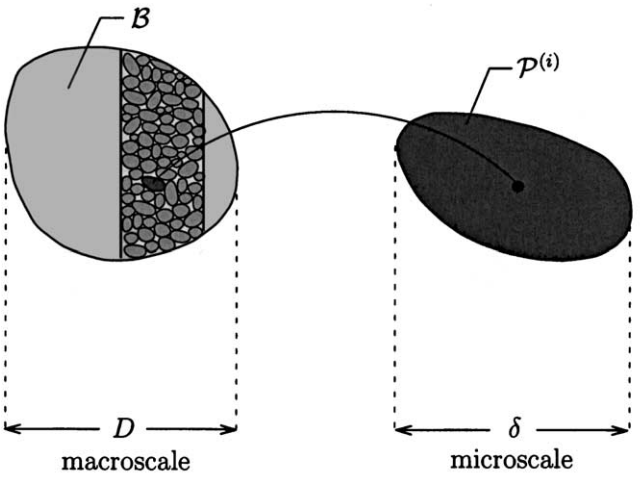

Fig. 2. Continuous body $\mathscr{B}$ consisting of a manifold of individual particles $\mathscr{P}^{(i)}$.

scale separation. Taking into account that the volume of the particles decreases with order $O(\varepsilon^3)$, while their surfaces only decrease with order $O(\varepsilon^2)$, it is easily concluded that, in the limiting case of small particles embedded in a large ensemble $\mathscr{B}$, where the scale ε tends to zero ($\varepsilon \to 0$), the volume terms in the momentum balance (8) or in the angular momentum balance (26) vanish and the general balance relations of the individual particles reduce to the equilibrium conditions of forces

$$\mathbf{0} = \mathbf{k} = \int_{\partial\mathscr{P}^{(i)}} \mathbf{t}\,\mathrm{d}a = \int_{\mathscr{P}^{(i)}} \operatorname{div}\mathbf{T}\,\mathrm{d}v \tag{36}$$

and of moments

$$\mathbf{0} = \mathbf{m}_0 = \int_{\partial\mathscr{P}^{(i)}} \mathbf{x}\times\mathbf{t}\,\mathrm{d}a = \int_{\mathscr{P}^{(i)}} \operatorname{div}\mathbf{M}\,\mathrm{d}v. \tag{37}$$

Following the arguments given in (27)–(30) again yields a symmetric stress

$$\mathbf{T} = \mathbf{T}^{\mathrm{T}} \tag{38}$$

on the particle level δ.

If the discussion concerns rigid particles, where the contact zones between the individual grains $\mathscr{P}^{(i)}$ are small in comparison to the whole particle surfaces $\partial\mathscr{P}^{(i)}$, one is allowed to assume point contacts rather than area contacts. Thus, the contact forces can be given as single forces $\mathbf{f}^{(i)c}$ acting at the contact points c, cf. Fig. 3, which are connected with the mass centers $\mathscr{M}^{(i)}$ of $\mathscr{P}^{(i)}$ by the branch vectors $\mathbf{l}^{(i)c}$.

Following this, the equilibrium conditions (36) and (37) can be given both in their continuous and in their discrete forms via

$$\mathbf{0} = \int_{\partial\mathscr{P}^{(i)}} \mathbf{t}\,\mathrm{d}a = \sum_{c=1}^{N} \mathbf{f}^{(i)c} \tag{39}$$

and

$$\mathbf{0} = \int_{\partial\mathscr{P}^{(i)}} \bar{\mathbf{x}}\times\mathbf{t}\,\mathrm{d}a = \sum_{c=1}^{N} \mathbf{l}^{(i)c}\times\mathbf{f}^{(i)c}, \tag{40}$$

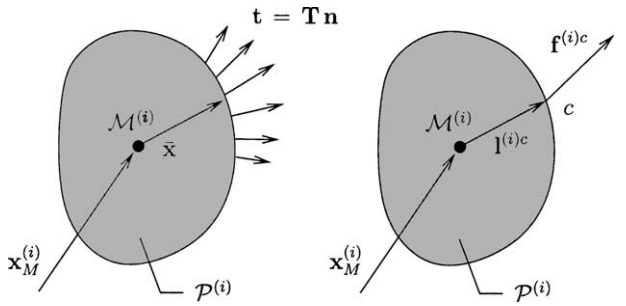

Fig. 3. Idealization of contact stresses to single contact forces.

where, to obtain (40) from (37), $\mathbf{x} = \mathbf{x}_M + \bar{\mathbf{x}}$ together with (39) has been used. Furthermore, it has been assumed that $\mathscr{P}^{(i)}$ is affected by N discrete contacts.

4. Embedded ensembles of particles

If the scale difference between the grains (microscale) on the one hand and the whole body (macroscale) on the other hand is sufficiently large, a mesoscale consisting of an ensemble of particles can be introduced in the sense of a REV. Following this, a standard continuum, which is generally understood to consist of a manifold of abstract material points, is now understood to consist of a manifold of REVs. Thus, the arguments of scale separation can be twicely applied, namely, when the REV is constructed as a manifold of grains by linking the micro- to the mesoscale and, furthermore, when the body is constructed as a manifold of REVs, i.e., when the mesoscale is linked to the macroscale, cf. Fig. 4. This situation, where three scales are touched, is well known as Hashin's MMM (micro–meso–macro) principle of homogenization (Hashin, 1983), which is intensively discussed with respect to the definition of the REV, e.g., by Bear and Bachmat (1991) or by Nemat-Nasser and Hori (1999). In particular, while the macroscopic scale is still of order $\mathrm{O}(D)$ and the microscopic scale is still of order $\mathrm{O}(\delta)$, the intermediate mesoscale of the REV is of order $\mathrm{O}(d)$.

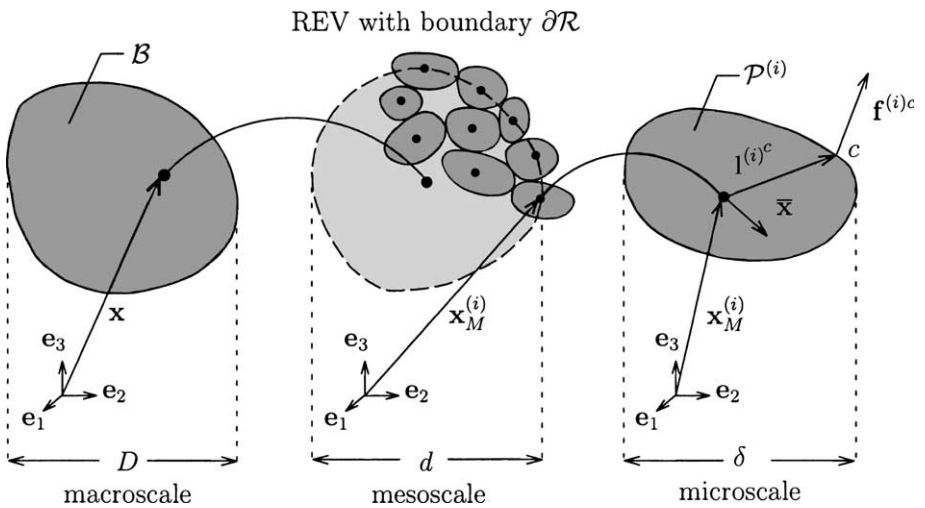

Fig. 4. Continuous body $\mathscr{B}$ consisting of particle ensembles (REVs).

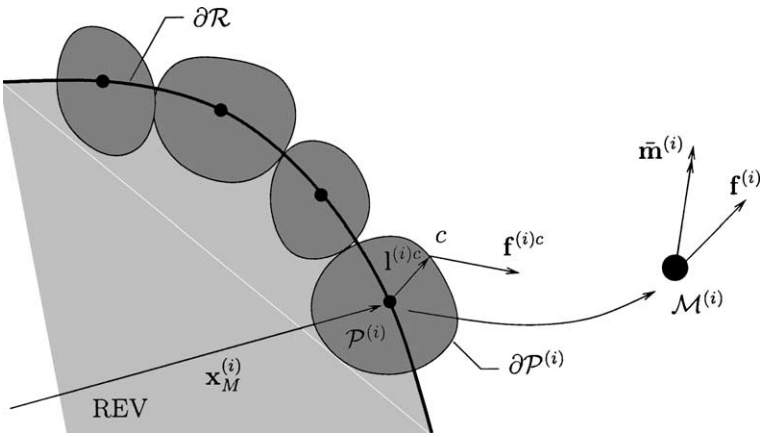

Fig. 5. Boundary of the REV, boundary particles with contact forces, force resultants and moment resultants.

Following the scale separation arguments, it is one of the key points of this article to assume that the position vectors $\mathbf{x}_M^{(i)}$ of the mass centers $M^{(i)}$ of the individual particles $\mathscr{P}^{(i)}$ with boundary $\partial\mathscr{P}^{(i)}$ can be understood as field quantities $\mathbf{x}_M$ in the REV with boundary $\partial\mathscr{R}$. Thus, the boundary of the REV is represented by the mass centers of the bounding particles, cf. Figs. 4 and 5. Furthermore, the scale separation arguments imply that the motion of the particles in the REV takes place on the scale $\varepsilon_\delta = \delta/d$, while the REV deforms in $\mathscr{B}$ on the scale $\varepsilon_d = d/D$. Assuming ε_δ and ε_d to be sufficiently small, i.e., $\varepsilon_\delta \ll 1$ and $\varepsilon_d \ll 1$, the simplified balance equations (36) and (37) of the grains hold in the REV and, furthermore, equivalent relations of the REV hold in $\mathscr{B}$. Thus, on the grain level, one has

$$\int_{\partial\mathscr{P}^{(i)}} \mathbf{t}\,\mathrm{d}a = \mathbf{0} \quad \text{and} \quad \mathbf{x}_M \times \int_{\partial\mathscr{P}^{(i)}} \mathbf{t}\,\mathrm{d}a + \int_{\partial\mathscr{P}^{(i)}} \bar{\mathbf{x}} \times \mathbf{t}\,\mathrm{d}a = \mathbf{0}, \tag{41}$$

while, on the REV level, it follows that

$$\int_{\partial\mathscr{R}} \mathbf{t}\,\mathrm{d}a = \mathbf{0} \quad \text{and} \quad \int_{\partial\mathscr{R}} (\mathbf{x}_M \times \mathbf{t} + \bar{\mathbf{x}} \times \mathbf{t})\,\mathrm{d}a = \mathbf{0}. \tag{42}$$

Given (42), it is evident from the character of the REV that the magnitude of the norms of $\mathbf{x}_M$ and of $\bar{\mathbf{x}}$ are of different size. Following this basically interprets $\bar{\mathbf{x}} \times \mathbf{t}$ as the fluctuations of $\mathbf{x}_M \times \mathbf{t}$, comparable to the turbulence contributions to the fluid stresses. Furthermore, note in passing that, in addition to Hashin's MMM principle, where $D \gg d \gg \delta$ leads to $\varepsilon \ll 1$, $\varepsilon_d \ll 1$ and $\varepsilon_\delta \ll 1$, the existence of non-vanishing fluctuations also implies that $\varepsilon_d \ll \varepsilon_\delta$.

Furthermore, substituting the moment $\bar{\mathbf{x}} \times \mathbf{t}$ by the notion $\bar{\mathbf{m}}$ and following the arguments of (24)–(26) or of (31)–(33), respectively, the REV balance relations (42) yield

$$\begin{aligned} &\int_{\partial\mathscr{R}} \mathbf{t}\,\mathrm{d}a = \int_{\mathscr{R}} \mathrm{div}_M \mathbf{T}\,\mathrm{d}v = \mathbf{0}, \\ &\int_{\partial\mathscr{R}} (\mathbf{x}_M \times \mathbf{t} + \bar{\mathbf{m}})\,\mathrm{d}a = \int_{\mathscr{R}} \mathrm{div}_M (\mathbf{M} + \overline{\mathbf{M}})\,\mathrm{d}v = \mathbf{0}, \end{aligned} \tag{43}$$

where $\mathrm{div}_M(\cdot)$ is the divergence operator with respect to the field $\mathbf{x}_M$ and, in extension of (33), $\bar{\mathbf{m}}$ is related to the couple stress $\overline{\mathbf{M}}$ using Cauchy's theorem via

$$\overline{\mathbf{M}} = \bar{\mathbf{x}} \times \mathbf{T} \rightarrow \bar{\mathbf{m}} = \overline{\mathbf{M}}\mathbf{n} = (\bar{\mathbf{x}} \times \mathbf{T})\mathbf{n} = \bar{\mathbf{x}} \times \mathbf{t}. \tag{44}$$

Given (43), the corresponding local statements read

$$\operatorname{div}_M \mathbf{T} = \mathbf{0}, \quad \operatorname{div}_M (\mathbf{M} + \overline{\mathbf{M}}) = \mathbf{0}. \tag{45}$$

If one furthermore splits the divergence of the stress moment $\mathbf{M}$ via (28) into

$$\operatorname{div}_M \mathbf{M} = \mathbf{I} \times \mathbf{T} + \mathbf{x}_M \times \operatorname{div}_M \mathbf{T}, \tag{46}$$

(45) and (46) combine to

$$\mathbf{I} \times \mathbf{T} + \operatorname{div}_M \overline{\mathbf{M}} = \mathbf{0}. \tag{47}$$

In contrast to (38) implying symmetric Cauchy stresses $\mathbf{T}$ on the particle level, it is found that $\mathbf{T}$ is non-symmetric on the level of the REV, whenever couple stresses $\overline{\mathbf{M}}$ occur. Furthermore, it is easily concluded from the definition of $\overline{\mathbf{M}}$ given by (44) that $\overline{\mathbf{M}}$ vanishes with vanishing fluctuations $\bar{\mathbf{x}} \times \mathbf{t}$, i.e., in the limit of vanishing $\bar{\mathbf{x}}$ with $|\bar{\mathbf{x}}| \to 0$. These arguments clearly show that the REV represents a micropolar Cosserat continuum, whenever $\overline{\mathbf{M}}$ exists, and that it has the character of a standard non-polar continuum in the limit of vanishing $\bar{\mathbf{x}}$. Furthermore, if the REV is considered as a continuum in the sense that it consists, theoretically, of a manifold of material points or particles, respectively, no matter whether or not $|\bar{\mathbf{x}}|$ tends to zero, the number of boundary particles is independent of the size of $|\bar{\mathbf{x}}|$ and the continuum can be considered, depending on the necessities of the model under consideration, either as a micropolar material or as a non-polar one.

On the other hand, realistic REVs consist of a certain number of grains instead of a theoretical manifold of material points. Thus, considering constant values of $|\bar{\mathbf{x}}|$, a transition from a Cosserat to a standard continuum can also be guaranteed. In this case, the REV volume has to be increased such that the ratio between the REV radius and the particle radius increases with an increasing ratio between the REV volume and the REV surface. Otherwise, the character of a Cosserat continuum is maintained.

If one is interested in the description of rigid particles embedded in the REV, the continuous formulation of the statements given above can be substituted by discrete statements, cf. (39) and (40). In this case, where the boundary of the REV is assumed to consist of B rigid particles $\mathscr{P}^{(i)}$, where each $\mathscr{P}^{(i)}$ has N° outward oriented discrete contacts, cf. Fig. 5, the force equilibrium statement $(43)_1$ on the REV level reads

$$\int_{\partial \mathscr{R}} \mathbf{t}\, \mathrm{d}a = \int_{\mathscr{R}} \operatorname{div}_M \mathbf{T}\, \mathrm{d}v = \sum_{i=1}^{B} \sum_{c=1}^{N^\circ} \mathbf{f}^{(i)c} = \sum_{i=1}^{B} \mathbf{f}^{(i)} = \mathbf{0}, \tag{48}$$

where the force resultants of the outward oriented contact forces acting on the boundary of the bounding particles $\mathscr{P}^{(i)}$ are given by

$$\mathbf{f}^{(i)} = \sum_{c=1}^{N^\circ} \mathbf{f}^{(i)c}. \tag{49}$$

Note in passing that the force resultants $\mathbf{f}^{(i)}$ represent the contact forces acting on the boundary $\partial \mathscr{P}$ of the REV. In addition to the force equilibrium statement, the equilibrium equation of moments on the REV level represented by $(43)_2$ turns out to yield

$$\begin{aligned} \int_{\partial \mathscr{R}} (\mathbf{x}_M \times \mathbf{t} + \bar{\mathbf{m}})\, \mathrm{d}a &= \int_{\mathscr{R}} \operatorname{div}_M (\mathbf{M} + \overline{\mathbf{M}})\, \mathrm{d}v = \sum_{i=1}^{B} \left(\mathbf{x}_M^{(i)} \times \mathbf{f}^{(i)} + \sum_{c=1}^{N^\circ} \mathbf{l}^{(i)c} \times \mathbf{f}^{(i)c} \right) \\ &= \sum_{i=1}^{B} (\mathbf{x}_M^{(i)} \times \mathbf{f}^{(i)} + \bar{\mathbf{m}}^{(i)}) = \mathbf{0}, \end{aligned} \tag{50}$$

where the resultants $\bar{\mathbf{m}}^{(i)}$ of the moments of the outward oriented contact forces acting on the bounding particles $\mathscr{P}^{(i)}$ and taken with respect to particle centers $M^{(i)}$ are given by

$$\bar{\mathbf{m}}^{(i)} = \sum_{c=1}^{N^\circ} \mathbf{l}^{(i)c} \times \mathbf{f}^{(i)c}. \tag{51}$$

Again, note in passing that the resulting moments $\bar{\mathbf{m}}^{(i)}$ represent the contact (Cosserat) moments acting on the boundary $\partial\mathscr{R}$ of the REV. Furthermore, it should be noticed that these moments are independent of the resulting forces $\mathbf{f}^{(i)}$. In contrast to the image of a continuous body, where the abstract assumption $|\bar{\mathbf{x}}| \to 0$ led from a micropolar to a non-polar continuum, a limit analysis in the frame of particle ensembles constituting the REVs generally exhibits non-vanishing moments $\bar{\mathbf{m}}^{(i)}$. Given realistic REVs with constant reference volume, this result is due to the fact that, even if the particle size $|\mathbf{l}^{(i)c}|$ on the microscale with order δ is extremely small such that $|\mathbf{l}^{(i)c}|/d \to 0$ on the mesoscale of the REV with order d, the number B of the particles bounding the REV tends to infinity, whenever the REV size does not shrink with the particle size. Thus, one generally obtains

$$\lim_{\substack{B\to\infty \\ |\mathbf{l}^{(i)c}|/d\to 0}} \sum_{i=1}^{B} \sum_{c=1}^{N^\circ} \mathbf{l}^{(i)c} \times \mathbf{f}^{(i)c} \neq \mathbf{0}. \tag{52}$$

As a consequence, the information of the discrete microstructure of the REV is embedded into a resulting continuum theory, where the material points are identified with the REVs. This continuum obviously turns out to be a micropolar Cosserat continuum (Diebels and Ehlers, 2001; Diebels et al., 2001; Ehlers et al., 2001a,b).

5. Homogenization strategy

Proceeding from the scale separation arguments by use of the MMM principle given in the previous section, the distribution of contact forces on the particle level can be replaced by stresses and couple stresses on the mesoscale of the REV. Similar arguments can be found in the literature, when the particle scale is related to the macroscale by homogenization, cf., e.g., the work by Drescher and de Josselin de Jong (1972), Cundall et al. (1982), Chang and Liao (1990), Bagi (1996) and Kruyt and Rothenburg (1998). Furthermore, embedding the REV in a body $\mathscr{B}$ yields the macroscopic stress and couple stress quantities at a material point of $\mathscr{B}$ as the homogenized counterparts of the REV stresses and couple stresses obtained by volume averaging procedures. Since the REVs are embedded in $\mathscr{B}$, the scale separation argument led to the local equilibrium conditions (45) on the REV level, where the stresses $\mathbf{T}$ and the stress moments $\mathbf{M} + \overline{\mathbf{M}}$ can both be replaced by an abstract substitute $\mathbf{A}$. Thus,

$$\operatorname{div}_M \mathbf{A} = \mathbf{0}. \tag{53}$$

Defining the macroscopic stress and couple stress tensors as volume averages $\langle\mathbf{A}\rangle$ taken over the REV yields (Hill, 1963)

$$\langle\mathbf{A}\rangle := \frac{1}{V_R} \int_{\mathscr{R}} \mathbf{A}\, \mathrm{d}v, \tag{54}$$

where V_R is the volume of the REV under consideration. In order to relate the average $\langle\mathbf{A}\rangle$ to the resultant forces and moments acting on the boundary of the REV, the following identities are needed:

$$\begin{aligned} &\mathbf{A}^{\mathrm{T}} = \mathbf{I}\mathbf{A}^{\mathrm{T}} = (\operatorname{grad}_M \mathbf{x}_M)\mathbf{A}^{\mathrm{T}}, \\ &\operatorname{div}_M(\mathbf{x}_M \otimes \mathbf{A}) = (\operatorname{grad}_M \mathbf{x}_M)\mathbf{A}^{\mathrm{T}} + \mathbf{x}_M \otimes \operatorname{div}_M \mathbf{A}. \end{aligned} \tag{55}$$

Combination of the above identities yields

$$\mathbf{A}^{\mathrm{T}} = \operatorname{div}_M(\mathbf{x}_M \otimes \mathbf{A}) - \mathbf{x}_M \otimes \operatorname{div}_M \mathbf{A}. \tag{56}$$

Following this, the volume average $\langle \mathbf{A}^{\mathrm{T}} \rangle = \langle \mathbf{A} \rangle^{\mathrm{T}}$ reads

$$\langle \mathbf{A} \rangle^{\mathrm{T}} = \frac{1}{V_R} \int_{\mathscr{R}} \mathrm{div}_M (\mathbf{x}_M \otimes \mathbf{A}) \, \mathrm{d}v - \frac{1}{V_R} \int_{\mathscr{R}} \mathbf{x}_M \otimes \mathrm{div}_M \mathbf{A} \, \mathrm{d}v. \tag{57}$$

By consideration of the generalized equilibrium condition (53), the second term of (57) vanishes, and one finally obtains the relation

$$\langle \mathbf{A} \rangle^{\mathrm{T}} = \frac{1}{V_R} \int_{\partial\mathscr{R}} (\mathbf{x}_M \otimes \mathbf{A}) \mathbf{n} \, \mathrm{d}a, \tag{58}$$

where the volume integral has been substituted by a surface integral using an extended Gaussian theorem.

Substituting the abstract equilibrium quantity $\mathbf{A}$ by the stress $\mathbf{T}$ yields

$$\langle \mathbf{T} \rangle^{\mathrm{T}} = \frac{1}{V_R} \int_{\partial\mathscr{R}} (\mathbf{x}_M \otimes \mathbf{T}) \mathbf{n} \, \mathrm{d}a = \frac{1}{V_R} \int_{\partial\mathscr{R}} \mathbf{x}_M \otimes \mathbf{t} \, \mathrm{d}a, \tag{59}$$

where Cauchy's theorem has been used. Following this, one finally obtains the average stress as

$$\langle \mathbf{T} \rangle = \frac{1}{V_R} \int_{\partial\mathscr{R}} \mathbf{t} \otimes \mathbf{x}_M \, \mathrm{d}a. \tag{60}$$

Furthermore, by substituting the local stresses by the particle stress resultants of the outward oriented contact forces given by (49) and by replacing the field quantities $\mathbf{x}_M$ by the position vectors $\mathbf{x}_M^{(i)}$ of the particle centers, one obtains the discrete relation

$$\langle \mathbf{T} \rangle = \frac{1}{V_R} \sum_{i=1}^{B} \mathbf{f}^{(i)} \otimes \mathbf{x}_M^{(i)}. \tag{61}$$

The above equation represents the well-known result that the average REV stress is given by the product of the contact forces (represented by the external force resultants acting on the boundary particles) and the branch vectors (related to the position vectors $\mathbf{x}_M^{(i)}$ of the mass centers of the boundary particles). However, note in passing that $\langle \mathbf{T} \rangle$ is generally non-symmetric with respect to the existence of couple stresses.

Substituting the abstract equilibrium quantity $\mathbf{A}$ by the stress moments $\mathbf{M}$ and the couple stresses $\overline{\mathbf{M}}$ yields in analogy to (59)

$$\langle \mathbf{M} + \overline{\mathbf{M}} \rangle^{\mathrm{T}} = \frac{1}{V_R} \int_{\partial\mathscr{R}} [\mathbf{x}_M \otimes (\mathbf{M} + \overline{\mathbf{M}})] \mathbf{n} \, \mathrm{d}a = \frac{1}{V_R} \int_{\partial\mathscr{R}} \mathbf{x}_M \otimes (\mathbf{x}_M \times \mathbf{t}) \, \mathrm{d}a + \frac{1}{V_R} \int_{\partial\mathscr{R}} \mathbf{x}_M \otimes \bar{\mathbf{m}} \, \mathrm{d}a, \tag{62}$$

where, $(44)_2$ together with

$$\mathbf{M}\mathbf{n} = (\mathbf{x}_M \times \mathbf{T}) \mathbf{n} = \mathbf{x}_M \times \mathbf{t} \tag{63}$$

has been used. Separating (62) by reasons yields

$$\begin{aligned} \langle \mathbf{M} \rangle &= \frac{1}{V_R} \int_{\partial\mathscr{R}} (\mathbf{x}_M \times \mathbf{t}) \otimes \mathbf{x}_M \, \mathrm{d}a, \\ \langle \overline{\mathbf{M}} \rangle &= \frac{1}{V_R} \int_{\partial\mathscr{R}} \bar{\mathbf{m}} \otimes \mathbf{x}_M \, \mathrm{d}a. \end{aligned} \tag{64}$$

Furthermore, by substituting the local stress and couple stress moments in analogy to (50) by the outward oriented contact forces acting on the boundary particles and substituting $\mathbf{x}_M$ by $\mathbf{x}_M^{(i)}$ and $\bar{\mathbf{m}}$ by the particle couples $\bar{\mathbf{m}}^{(i)}$, one obtains

$$\begin{aligned}\langle \mathbf{M} \rangle &= \frac{1}{V_R} \sum_{i=1}^{B} (\mathbf{x}_M^{(i)} \times \mathbf{f}^{(i)}) \otimes \mathbf{x}_M^{(i)}, \\ \langle \overline{\mathbf{M}} \rangle &= \frac{1}{V_R} \sum_{i=1}^{B} \bar{\mathbf{m}}^{(i)} \otimes \mathbf{x}_M^{(i)}.\end{aligned} \tag{65}$$

Finally, the identity

$$(\mathbf{a} \times \mathbf{b}) \otimes \mathbf{c} = \mathbf{a} \times (\mathbf{b} \otimes \mathbf{c}) \tag{66}$$

of tensor calculus, valid for arbitrary vectors $\mathbf{a}$, $\mathbf{b}$, $\mathbf{c}$, together with the definition of the particle couples $\bar{\mathbf{m}}^{(i)}$ from (51) yields

$$\begin{aligned}\langle \mathbf{M} \rangle &= \frac{1}{V_R} \sum_{i=1}^{B} \mathbf{x}_M^{(i)} \times (\mathbf{f}^{(i)} \otimes \mathbf{x}_M^{(i)}), \\ \langle \overline{\mathbf{M}} \rangle &= \frac{1}{V_R} \sum_{i=1}^{B} \left(\sum_{c=1}^{N^\circ} \mathbf{l}^{(i)c} \times \mathbf{f}^{(i)c} \right) \otimes \mathbf{x}_M^{(i)}.\end{aligned} \tag{67}$$

From the above results, it is seen that the stress moment $\langle \mathbf{M} \rangle$ is given as the sum of the moments of the stress contributions included in $\langle \mathbf{T} \rangle$ from (61), while the couple stress $\langle \overline{\mathbf{M}} \rangle$ is obtained similar to (61), when the stress contributions $\mathbf{f}^{(i)}$ of the bounding particles included in (61) are substituted by the sum of the particle contact moments included in $\bar{\mathbf{m}}^{(i)}$ from (51). Furthermore, it is concluded that a couple stress exists, whenever the MMM principle is applied to particle ensembles embedded in a continuous medium. The couple stress results from the fact that a mesoscopic REV consisting of an ensemble of microscopic particles has been embedded in a macroscopic body, which is clearly obtained as a micropolar Cosserat continuum with considerable values of $\overline{\mathbf{M}}$, if $\varepsilon_d \ll \varepsilon_\delta$ holds in addition the MMM principle. It has furthermore been shown, on the one hand, that the character of micropolarity is maintained even in case of decreasing particle sizes as far as the REV size does not decrease in the same manner, cf. (52). On the other hand, it is furthermore concluded that, if the REV decreases to the particle size, e.g., if the REV can be identified by a single particle, the stress becomes symmetric, cf. (38), and the Cosserat continuum changes towards a standard non-polar continuum.

Applying the above results to continuum mechanical problems implies that the stresses incorporated in (9) as well as the stresses and the couple stresses incorporated in $(35)_2$ can be replaced by the above averages $\langle \mathbf{T} \rangle$ and $\langle \overline{\mathbf{M}} \rangle$. Finally, if a standard continuum is concerned, e.g., in frame of the FEM, one has to solve only the weak form of the momentum balance (9), while, if a micropolar continuum has to be considered, one has to solve the weak form of (9) together with the weak form of the angular momentum balance $(35)_2$, cf. Ehlers (2002). On the other hand, if one is interested to fully solve the problem on the particle level, e.g., by use of the DEM, one has to solve the Eulerian equations (7) and $(22)_2$ for each particle taking into account convenient contact conditions. Based on solutions of the discrete problem, arbitrary sizes of REVs can be investigated in order to study the homogenization process yielding the local averages $\langle \mathbf{T} \rangle$ and $\langle \overline{\mathbf{M}} \rangle$.

6. Numerical example and validation

In the present section, the homogenization procedure discussed above is applied to the boundary-value problem of the biaxial test, cf. Fig. 6. In particular, a two-dimensional problem is taken into account, where the biaxial box under consideration consists of a manifold of rigid grains. The computations are carried out in the framework of the DEM, where the appearance of asymmetric stresses accompanied by couple stresses is studied with respect to different REV sizes. Following this, the key focus concerns the question,

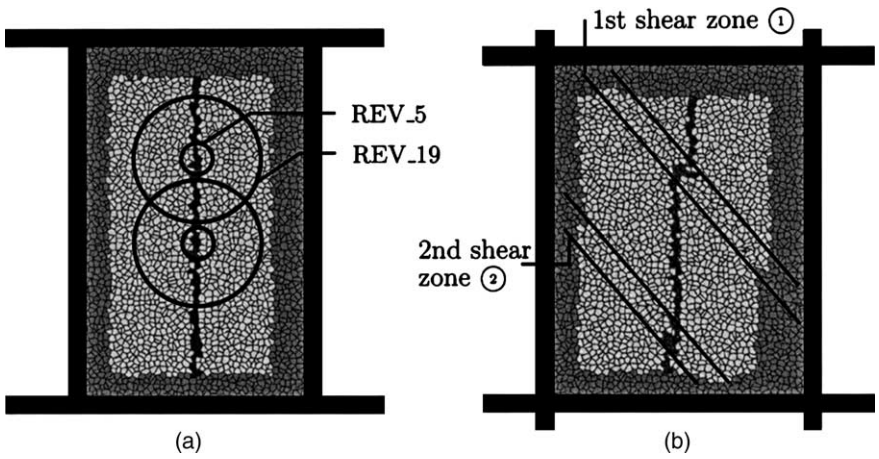

Fig. 6. Biaxial setup and deformed state of the benchmark under study.

how large must the REV be in order to yield, on the one hand, local averages as convenient substitutes of their microscopic counterparts and, on the other hand, a correct representation of the underlying microstructure. In particular, this question can be answered on the basis of how much particles have to be included within the REV such that the a.m. requirements can be satisfied. By numerical simulations, an "ideal" size of the REV on the mesoscale of order d can be discussed that guarantees a reliable quantitative comparability with the macroscale of order D without loss of locality.

6.1. Discrete element model

The following computations are carried out on the basis of a two-dimensional discrete element simulation (Cundall and Strack, 1979) with convex polygonal particles, cf. Tillemans and Herrmann (1995) and Kun and Herrmann (1996), representing, e.g., a dry granular material like sand, where each particle center is assigned three degrees of freedom, two translations and one rotation. Furthermore, the model is based on a particle composite, where the polygonal mesh is determined by a Voronoi tessellation considering the generated polygons as rigid grains. Following this, these grains are assumed to be neither breakable nor deformable, but they may overlap when they are pressed against each other. In addition, the local deformation behaviour caused by the overlaps can be approximated by elastic repulsive forces $\mathbf{f}^{(i)c}$ at each contact point c of a particle $\mathscr{P}^{(i)}$. In general, the repulsive forces can be related to the overlapping areas of the particles in contact with respect to both normal and tangential stiffnesses (Tillemans and Herrmann, 1995), which can be related to each other, e.g., by Coulomb's friction law. Furthermore, if more sophisticated models are of interest, additional rotational stiffnesses can be taken into account. In the present simulation, rotational stiffnesses as well as the tangential parts of the contact forces are neglected. However, this has not only been done for simplicity, but also in order to show that, in the case of polygonal grains, couple stresses simply arise from the eccentricities of the particle contacts with respect to the local mass centers and have not to be introduced by a refined contact description, where the transfer of moments additionally stems from tangential contact forces and rotational stiffnesses, cf., e.g. Chang and Liao (1990) and Chang and Gao (1995). The force resultants $\mathbf{f}^{(i)}$ and the moment resultants $\bar{\mathbf{m}}^{(i)}$, which are now only due to the eccentricities of the normal forces of each $\mathscr{P}^{(i)}$, are inserted into the equations of motion, which are numerically solved for each particle with the aid of the Gear–Predictor–Corrector time integration scheme, thus yielding the new positions, velocities and accelerations of the particles. More information on

the applied model as well as further descriptive simulation results can be found in D'Addetta et al. (2001, 2002).

6.2. The biaxial problem

In this article, the benchmark used for the validation of the above homogenization procedure is chosen as a strain driven biaxial simulation, where the biaxial box with rigid side walls consists of approximately 2500 polygonal particles. Loading takes place by pressing together the top and bottom platens with a constant velocity, while the side walls are assigned a constant pressure, cf. Fig. 6. While it is well known from experiments on granular samples that a shear localization occurs at a certain amount of vertical displacements (Viggiani et al., 2001), it has additionally been found by numerical simulations based on a Cosserat continuum included in the FEM (Ehlers and Volk, 1998) that the localization zone is affected by micropolar rotations and couple stresses, while, in the remainder of the biaxial domain, no Cosserat rotations or couple stresses occur. Following this, it is easily concluded that the micropolar effects occurring in the boundary-value problem under study are of boundary layer type. These results are not only expected to be recovered by use of the DEM, but it is also expected that the homogenization process detects the macroscopic couple stresses $\overline{\mathbf{M}}$ in the shear band zones by taking suitable volume averages over REVs in the localizing domains. Finally, it should be mentioned that the following study, although it is understood as an adequate benchmark for the validation of the proposed homogenization technique, does not allow for a quantitative comparison with a real granular structure, since the parameters and contact laws, which are used here, are chosen arbitrarily.

In Fig. 6(a), the initial particle structure of the biaxial problem is presented. The particles on the vertical middle line of the sample are darkened in order to simplify a comparison with the deformed state given in Fig. 6(b). Furthermore, two center particles, each belonging to two different REV sizes, are marked. These REVs, which are widely used in the following homogenization procedure, are compared to each other when they are assumed to exhibit idealized diameter of either five particles (REV_5) or of 19 particles (REV_19). The deformed sample, cf. Fig. 6(b), shows the formation of two parallel shear zones, where the upper one ① appeared firstly. Note in passing that the particles above the shear zone ① and below the shear zone ② form wedges that undergo a rigid body translation without any visible internal deformation or rotation. The region in between the shear zones behaves like a rectangular block sheared at the top and at the bottom. Between the wedges and the middle block, regions of finite width with high shear rates characterized by dilation and particle rotations represent the shear bands. As can be seen by a comparison of the accentuated particles before and after the deformation of the specimen, the deformation of the sample is highly localized in the shear band domains. The purely local deformation of the vertical line of the darkened particles reveals a reorganization of the particle structure. In particular, this line remains vertical, except of the "discontinuity" in the region of the shear zones. Although a comparison with experimental data is not the topic of the present contribution, it should be emphasized that the simulations given here are in good qualitative agreement with both experimental and numerical results of dry granular materials like sand etc., cf. the biaxial experiments on Hostun sand given by Viggiani et al. (2001) or the computations described by Ehlers and Volk (1998).

6.3. Numerical results

At each time step of the biaxial simulation, the average stress and couple stress tensors according to (61) and $(67)_2$ have been evaluated for approximately 1500 REVs. These REVs have been created in the following way, cf. D'Addetta et al. (2003): After having drawn a circle around the center particle of the REV under consideration, all particles inside the circle and those boundary particles with mass centers inside the circle are assumed to belong to the REV. Following this, the polygonal line following the mass centers of

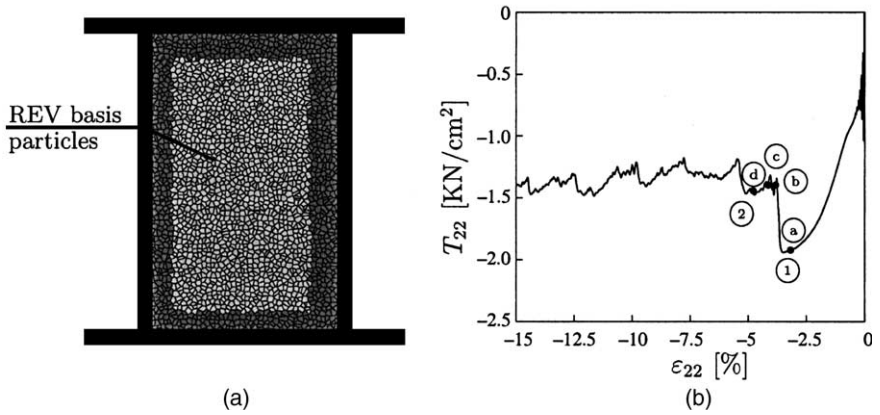

Fig. 7. REV basis particles (a) and "macroscopic" stress–strain behaviour (b).

the bounding particles represents the boundary $\partial\mathscr{R}$ of the REV with the volume V_R. The composition of each REV is fixed at the beginning of the simulation and is not changed in the course of it. One could think of all particles within the REVs that they are surrounded by a flexible vessel allowing for internal deformation as well as for an interchange of forces with the surrounding particles (Huet, 1997). Hence, the shape of the REVs can only be coarsely approximated by a circle, cf. Fig. 6(a) for two arbitrarily chosen REV positions. The basis particles (centers) of all controlled REVs are the lightened particles shown in Figs. 6 and 7(a), where, around each of those particles, a more or less circular influence region defines the REV.

Different REV sizes have been investigated in order to verify the proposed homogenization technique. Throughout this section, the focus lies on the following two REV sizes:

- REV_5: On average, there is a REV diameter of five particles with approximately 20 particles inside the REV,
- REV_19: On average, there is a REV diameter of 19 particles with approximately 280 particles inside the REV.

In Fig. 7(b), the overall stress–strain response in terms of the vertical coefficient T_{22} of the stress tensor $\mathbf{T}$ is plotted versus the strain coefficient ε_{22}. Therein, T_{22} refers to the externally measurable stress answer of the sample computed by the reaction forces at the bottom or the top loading platens divided by the sample areas. Furthermore, ε_{22} is simply measured by the vertical displacement with respect to the specimen height. The pointers ① and ② at the stress–strain curve denote the evolution of the shear bands emphasized in Fig. 6(b). Due to the formation of the first shear band in the upper part of the sample, cf. ①, a sharp drop by 25% of the stress is achieved. When the second shear band occurs at ② a short time later, a further but smaller drop of the stress is observed. Afterwards, the deformation of the sample continues without any notable increase of stress. Note in passing that the consideration of polygonal particles instead of circular ones prevents from the formation of rolling modes within the particle sample, typically seen in simulations with circles, cf. Ehlers et al. (2001a,b). Furthermore, at pointer ①, the typical particle interlock for polygonally shaped grains ends up in an abrupt failure, when suddenly a part of the stored energy is set free.

The goal of the further computations is to show that the application of the above homogenization technique maintains inhomogeneous effects occurring on the microscale when the microstructure is transferred towards the mesoscopic REV. However, this statement depends on the chosen REV size. To illustrate this statement, two particular REV positions are used for the oncoming comparison. In the first case, the corresponding REV basis particle lies within the firstly evolving shear band, whereas, in the second

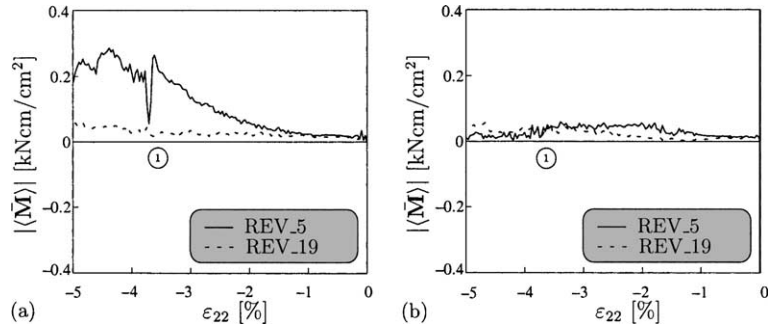

Fig. 8. Norm of the couple stress tensor $\langle\overline{\mathbf{M}}\rangle$ for different REVs inside (a) the shear band ① and outside (b) the evolving shear bands.

case, the basis particle is situated outside of the influence zone of both shear bands. Both basis particles are identified with the centers of the circles marked in Fig. 6(a). In Fig. 8, the norm $|\langle\overline{\mathbf{M}}\rangle| = \sqrt{\langle\overline{M}_{13}\rangle^2 + \langle\overline{M}_{23}\rangle^2}$ of the couple stress tensor $\langle\overline{\mathbf{M}}\rangle$ corresponding to the REV sizes REV_5 and REV_19 at the two REV positions is plotted versus the nominal vertical strain coefficient ε_{22} defined above. Concerning Fig. 8, two effects are visible: Firstly, as has been expected, couple stresses are only active in the shear band zone, cf. Fig. 8(a), while outside the shear band no couple stresses occur, cf. Fig. 8(b). Secondly, the homogenized couple stresses become only visible if the REV size is small enough such that microscopic effects are not smeared out on the mesoscale, cf. the different results of REV_5 and REV_19 given in Fig. 8(a). Once again, these observations are in good agreement with both numerical simulations carried out on the basis of the FEM by use of a micropolar Cosserat continuum (Ehlers and Volk, 1998; Ehlers, 2002) as well as experimental results on dry granular materials. Since the width of experimentally observable shear bands, like in sand, consists of only a few grain diameters (Viggiani et al., 2001), a REV should not be chosen too large in order to capture the influence of the microscopic inhomogeneities on the macroscale. In Figs. 8 and 9, the pointer ① again indicates the onset of the first shear band.

Concerning the particle contact behaviour included in this study, recall that only normal stiffnesses have been taken into account and that tangential forces as well as rotational stiffnesses have not been considered. Thus, in contrast to articles, where rotational stiffnesses are used, cf., e.g., the work by Chang and Gao (1995), the couple stresses naturally result from the eccentricities of the normal contact forces and are neither due to tangential contact forces nor to an enhanced contact description through the introduction of rotational stiffnesses.

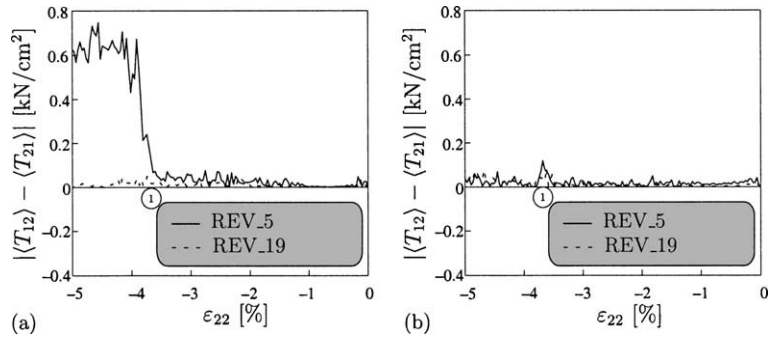

Fig. 9. Difference of shear stresses included in $\langle\mathbf{T}\rangle$ for different REVs inside (a) and outside (b) the evolving shear band.

In addition to the couple stresses, a further indicator for the existence of localization zones is the existence of non-symmetric stress tensors, which, in the biaxial problem under study, are given by non-vanishing differences between $\langle T_{12}\rangle$ and $\langle T_{21}\rangle$. Recall that, if a couple stress exists, the stress tensor is not symmetric and, hence, $\langle T_{12}\rangle \neq \langle T_{21}\rangle$ is expected to hold in the localization zone. In Fig. 9, the value $|\langle T_{12}\rangle - \langle T_{21}\rangle|$ of the difference between the shear stresses is plotted with respect to the size and the position of the REVs. From this figure, it is clearly seen when $\langle \mathbf{T}\rangle$ becomes unsymmetric. In analogy to the detection of couple stresses, it is evident that stress asymmetries are only obtained in the case of a sufficiently small REV lying within the localization region. Concerning the present example, there is only a clear difference between $\langle T_{12}\rangle$ and $\langle T_{21}\rangle$, cf. Fig. 9(a), for the REV with size REV_5 located inside the shear band. Furthermore, it is seen that the REV with size REV_19 is unable to detect a shear zone by use of the proposed homogenization technique. In addition, it is obvious that the REVs outside of the developing shear bands exhibit symmetric stresses like they exhibit vanishing couple stresses, cf. Figs. 8(b) and 9(b).

Concerning the above results, it should be mentioned that a $\langle T_{22}\rangle$ versus ε_{22} diagram of the corresponding REVs would principally follow the graph of the macroscopic stress–strain curve given in Fig. 7(b). Therein, the locality of the variables is included expressed by fluctuations in the $\langle T_{22}\rangle$ values with respect to the position of the REVs. Furthermore, it is observed that the amplitude of stress asymmetries decreases with increasing volumes of the REVs. These findings do not only correspond to the remarks given above in Section 4, but they are also related to the observations made by Bardet and Vardoulakis (2001). In addition to the findings by Bardet and Vardoulakis, the present article also provides a backbone for a sound numerical treatment of the proposed homogenization process. It has furthermore been found that the position as well as the size of the REVs play an important role, as stress asymmetries and, thus, couple stresses are only active in the shear band zones. Following this, the result of an averaging procedure strongly depends on the selection and on the geometry of the particular REV.

Finally, the temporal progress of the couple stresses as is shown in Figs. 10 and 11 gives additional insight into the activation of couple stresses in shear zones. The norm of the couple stress tensor is plotted for both REV sizes with respect to the time steps ⓐ, ⓑ, ⓒ and ⓓ indicated in Fig. 7(b). This sequence covers the time interval between the development of the first shear band and the onset of the second one. Note in passing that the deformation of the sample at time step ⓓ has already been presented in Fig. 6(b). Furthermore, the homogenized quantities computed for the particular REVs are projected onto the

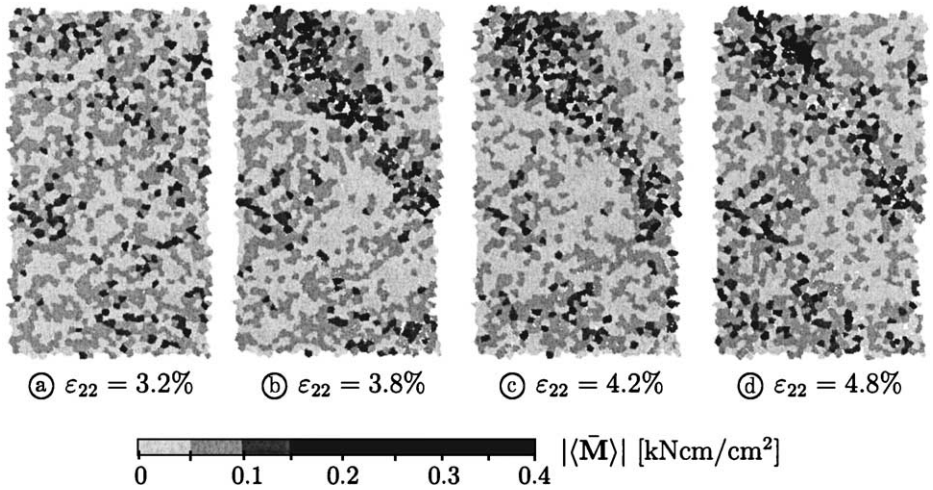

Fig. 10. Temporal progress of the norms of the couple stresses for REVs of size REV_5.

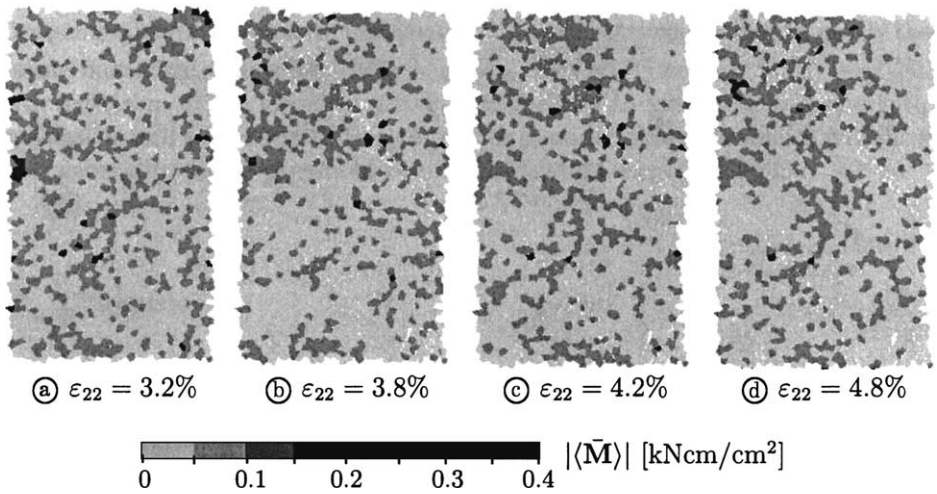

Fig. 11. Temporal progress of the norms of the couple stresses for REVs of size REV_19.

corresponding basis particle in the deformed state, where the increasing darkness of each basis particle represents the increasing average couple stress value in a circular neighbourhood of this particle. In addition, it should be mentioned that only those basis particles indicated by a light colour in Fig. 7(a) are used for the graphical representation of Figs. 10 and 11. Hence, no REVs have been placed in the boundary regions of the sample. A clear localization of the couple stresses becomes evident within the region of the firstly evolving shear band for the REVs of size REV_5. Moreover, different points of activity within the shear zone can be recognized during the course of the controlled time interval. This shows that the formation of the localization zone is not as abrupt as one could think when the overall stress–strain response in Fig. 7(b) is observed. In contrast, the temporal progress for REVs of size REV_19 does not reveal any activity within the first shear zone. This fact would become even more evident, if the scale in Fig. 11 would be adapted to the maximum values of REV_19. As a consequence of the relative large size of REV_19, the norm of the couple stresses tends to zero and a smearing-out effect is obtained. Nevertheless, small local fluctuations are still present, however, in a statistically distributed manner instead of a strict localization as was found for the REVs of size REV_5. A more detailed analysis of the boundary-value problem under study with emphasis on the numerical application of the presented homogenization strategy will be given in a follow-up paper (D'Addetta et al., 2003).

However, there exists the following general dilemma: On the one hand, a discrete model has been applied in contrast to a continuum model in order to precisely describe the locality of certain mechanical variables. On the other hand, macroscopic stresses and couple stresses are required and should be obtained by averaging or homogenization methods without yielding a loss of the detected locality. But, since each homogenization technique based on averaging includes a filter with respect to the computation of the relevant mechanical quantities, there is always the risk of losing the information to be investigated. Concerning this remark, it has been found within the present study that an "ideal" REV size was obtained by the size REV_5 containing around 20 particles. This REV, however far away from the theoretical requirement of a manifold of particles, was found to be large enough to correctly represent averages relating microscopic to macroscopic quantities and small enough to catch localization effects like couple stresses and stress asymmetries. Further on, the REV_5 size guarantees values of the average stress $\langle\mathbf{T}\rangle$ to be comparable to the results of a fully macroscopic analysis in the framework of a continuum model. Of course, considering the REV_5 size as "ideal" only holds for the problem under study, when the compu-

tation of stresses and couple stresses is concerned. This statement has been checked by additional computations, where the volume terms (body forces and accelerations) that are skipped by the homogenization procedure are included in the computations leading to nearly the same numerical values for $|\langle\overline{\mathbf{M}}\rangle| = \sqrt{\langle\overline{M}_{13}\rangle^2 + \langle\overline{M}_{23}\rangle^2}$ and for $|\langle T_{12}\rangle - \langle T_{21}\rangle|$. An extension of the ideas presented in this study to kinematic and energetic values, as well as the application to further boundary-value problems will show the generality of the presented results (D'Addetta et al., 2003).

7. Conclusions

The present contribution recalls the basic axioms of rigid body dynamics and of continuum mechanics as the basis for a homogenization procedure relating the contact forces between the grains of a particle ensemble to macroscopic stresses and couple stresses. Following the arguments of scale separation, the behaviour of embedded particles is governed by equilibrium conditions which are expressed in terms of force and moment resultants in the mass centers of the individual grains. Finally, volumetric averages yield expressions for the stresses and for the couple stresses. While the stresses are related to the forces acting on the particles, the couple stresses are related to the moments resulting from the reduction of the contact forces towards the particle mass centers.

The proposed homogenization strategy has been applied to a biaxial test simulated by the DEM. It has been found that the diameter of the REVs should be of the order of around 5 times the typical particle diameter in order to reproduce the macroscopic stress response together with localization effects occurring when strong inhomogeneities dominate the local behaviour. Increasing the diameter of the REVs leads to smearing out the results in the sense that localizations become invisible. In particular, it was found that micropolar effects occurring in the shear band zones are governed by the existence of couple stresses and non-symmetric stress tensors. These effects are of boundary layer type and are, therefore, only detected by sufficiently small REVs, while they are shrinking with increasing REV sizes. From the biaxial example under study, the thickness of the shear band was found to be of the order of only several grain diameters, thus limiting the REV size to about 5 particle diameters. Following this, the size of the REV is obviously limited by the size of the effects to be described rather than by the theoretical requirement of containing a "manifold" of particles. Finally, the presented results clearly show that a particle ensemble has the character of a micropolar Cosserat continuum rather than it represents a non-polar standard continuum.

Acknowledgement

The authors wish to thank the "Deutsche Forschungsgemeinschaft" (DFG) for the financial support given to the Research Group FOR 326 "*Modellierung kohäsiver Reibungsmaterialien*".

References

Bagi, K., 1996. Stress and strain in granular assemblies. Mechanics of Materials 22, 165–177.

Bardet, J.P., Vardoulakis, I., 2001. The asymmetry of stress in granular media. International Journal of Solids and Structures 38, 353–367.

Bear, J., Bachmat, Y., 1991. Introduction to Modeling of Transport Phenomena in Porous Media. Kluwer Academic Publishers, Dordrecht.

Brinkgreve, R.B.J., 1994. Geomaterial models and numerical analysis of softening. Ph.D. Thesis. CIP-Gegevens Koniglijke Bibliotheek, Den Haag.

Chang, C.S., Liao, C.L., 1990. Constitutive relation for a particulate medium with the effect of particle rotation. International Journal of Solids and Structures 26, 437–453.

Chang, C.S., Gao, J., 1995. Second-gradient constitutive theory for granular material with random packing structure. International Journal of Solids and Structures 32, 2279–2293.

Cundall, P.A., Strack, O.D.L., 1979. A discrete numerical model for granular assemblies. Géotechnique 29, 47–65.

Cundall, P.A., Drescher, A., Strack, O.D.L., 1982. Numerical experiments in granular assemblies; measurements and observations. In: Vermeer, P.A., Luger, H.J. (Eds.), IUTAM Conference on Deformation and Failure of Granular Materials, A.A. Balkema, Rotterdam, pp. 355–370.

D'Addetta, G.A., Kun, F., Herrmann, H.J., Ramm, E., 2001. From solids to granulates—Discrete element simulations of fracture and fragmentation processes in geomaterials. In: Vermeer, P.A., Diebels, S., Ehlers, W., Herrmann, H.J., Ramm, E. (Eds.), Continuous and Discontinuous Modelling of Cohesive-Frictional Materials. Springer-Verlag, Berlin, pp. 231–258.

D'Addetta, G.A., Kun, F., Herrmann, H.J., Ramm, E., 2002. On the application of a discrete model to the fracture process of cohesive granular materials. Granular Matter 4, 77–90.

D'Addetta, G.A., Ramm, E., Diebels, S., Ehlers, W., 2003. A particle center based homogenization strategy for granular assemblies. Engineering Computations, in press.

Diebels, S., Ehlers, W., 2001. Homogenization method for granular assemblies. In: Wall, W.A., Bletzinger, K.-U., Schweizerhof, K. (Eds.), Trends in Computational Mechanics. CIMNE, Barcelona, pp. 79–88.

Diebels, S., Ehlers, W., Michelitsch, T., 2001. Particle simulations as a microscopic approach to a Cosserat continuum. Journal de Physique IV France 11, 203–210.

Drescher, A., de Josselin de Jong, G., 1972. Photoelastic verification of a mechanical model for the flow of granular material. Journal of the Mechanics and Physics of Solids 20, 337–351.

Ehlers, W., 2002. Foundations of multiphasic and porous materials. In: Ehlers, W., Bluhm, J. (Eds.), Porous Media: Theory, Experiments and Numerical Applications. Springer-Verlag, Berlin, pp. 3–86.

Ehlers, W., Volk, W., 1998. On theoretical and numerical methods in the theory of porous media based on polar and non-polar elasto-plastic solid materials. International Journal of Solids and Structures 35, 4597–4617.

Ehlers, W., Diebels, S., Michelitsch, T., 2001a. Microscopic modelling of granular materials taking into account particle rotations. In: Vermeer, P.A., Diebels, S., Ehlers, W., Herrmann, H.J., Ramm, E. (Eds.), Continuous and Discontinuous Modelling of Cohesive-Frictional Materials. Springer-Verlag, Berlin, pp. 259–274.

Ehlers, W., Ellsiepen, P., Ammann, M., 2001b. Time- and space-adaptive methods applied to localization phenomena in empty and saturated micropolar and standard porous materials. International Journal for Numerical Methods in Engineering 52, 503–526.

Hashin, Z., 1983. Analysis of composite materials—a survey. ASME Journal of Applied Mechanics 50, 481–505.

Hill, R., 1963. Elastic properties of reinforced solids: some theoretical principles. Journal of the Mechanics and Physics of Solids 11, 357–372.

Huet, C., 1997. An integrated micromechanics and statistical continuum thermodynamics approach for studying the fracture behaviour of microcracked heterogeneous materials with delayed response. Engineering Fracture Mechanics 58, 459–556.

Kruyt, N.P., Rothenburg, L., 1998. Statistical theories for the elastic moduli of two-dimensional assemblies of granular materials. International Journal of Engineering Science 36, 1127–1142.

Kun, F., Herrmann, H.J., 1996. A study of fragmentation processes using a discrete element method. Computer Methods in Applied Mechanics and Engineering 138, 3–18.

Mühlhaus, H.-B., Vardoulakis, I., 1987. The thickness of shear bands in granular materials. Géotechnique 37, 271–283.

Nemat-Nasser, S., Hori, M., 1999. Micromechanics: Overall Properties of Heterogeneous Materials. Elsevier Science Publisher, Amsterdam.

Tillemans, H.-J., Herrmann, H.J., 1995. Simulating deformations of granular solids under shear. Physica A 217, 261–288.

Vardoulakis, I., Sulem, J., 1995. Bifurcation Analysis in Geomaterials. Blackie Academic and Professionals, London.

Viggiani, G., Küntz, M., Desrues, J., 2001. An experimental investigation of the relationships between grain size distribution and shear banding in sand. In: Vermeer, P.A., Diebels, S., Ehlers, W., Herrmann, H.J., Ramm, E. (Eds.), Continuous and Discontinuous Modelling of Cohesive-Frictional Materials. Springer-Verlag, Berlin, pp. 111–127.